CLEO CONF 95-09
EPS0165
July 24, 1995

MEASUREMENT OF BRANCHING RATIOS FOR EXCLUSIVE $b \to u\ell\nu$ DECAYS

The CLEO Collaboration

ABSTRACT

We have measured the branching ratio for $B \to \pi\ell\nu$ and for $B \to \rho\ell\nu$. B decays to the final states $\pi^{\mp}\ell^{\pm}\nu$, $\pi^0\ell^{\pm}\nu$, $\rho^{\mp}\ell^{\pm}\nu$, $\rho^0\ell^{\pm}\nu$ and $\omega\ell^{\pm}\nu$ are identified via full reconstruction, using a measurement of the missing energy and momentum in the event to infer the neutrino momentum. With a sample of 2.6×10^6 $B\bar{B}$ decays collected with the CLEO detector at CESR, and imposing the constraints $\frac{1}{2}\Gamma(B^0 \to \pi^-\ell^+\nu) = \Gamma(B^+ \to \pi^0\ell^+\nu)$ and $\frac{1}{2}\Gamma(B^0 \to \rho^-\ell^+\nu) = \Gamma(B^+ \to \rho^0\ell^+\nu) \approx \Gamma(B^+ \to \omega\ell^+\nu)$, we find branching ratios $\mathcal{B}(B^0 \to \pi^-\ell^+\nu) = (1.34 \pm 0.35 \pm 0.28) \times 10^{-4}$, and $\mathcal{B}(B^0 \to \rho^-\ell^+\nu) = (2.28 \pm 0.36 \pm 0.59^{+0.00}_{-0.46}) \times 10^{-4}$. The ratio of widths $\Gamma(B^0 \to \rho^-\ell^+\nu)/\Gamma(B^0 \to \pi^-\ell^+\nu) = 1.70^{+0.81}_{-0.50} \pm 0.58^{+0.00}_{-0.34}$. These results use the ISGW model for efficiencies. If instead one uses the WSB model, one finds $\mathcal{B}(B^0 \to \pi^-\ell^+\nu) = (1.63 \pm 0.46 \pm 0.34) \times 10^{-4}$, $\mathcal{B}(B^0 \to \rho^-\ell^+\nu) = (3.88 \pm 0.54 \pm 1.01^{+0.00}_{-0.78}) \times 10^{-4}$, and $\Gamma(B^0 \to \rho^-\ell^+\nu)/\Gamma(B^0 \to \pi^-\ell^+\nu) = 2.39^{+1.18}_{-0.69} \pm 0.81^{+0.00}_{-0.48}$.

R. Ammar,[1] P. Baringer,[1] A. Bean,[1] D. Besson,[1] D. Coppage,[1] N. Copty,[1] R. Davis,[1] N. Hancock,[1] S. Kotov,[1] I. Kravchenko,[1] N. Kwak,[1] Y. Kubota,[2] M. Lattery,[2] M. Momayezi,[2] J.K. Nelson,[2] S. Patton,[2] R. Poling,[2] V. Savinov,[2] S. Schrenk,[2] R. Wang,[2] M.S. Alam,[3] I.J. Kim,[3] Z. Ling,[3] A.H. Mahmood,[3] J.J. O'Neill,[3] H. Severini,[3] C.R. Sun,[3] F. Wappler,[3] G. Crawford,[4] R. Fulton,[4] D. Fujino,[4] K.K. Gan,[4] K. Honscheid,[4] H. Kagan,[4] R. Kass,[4] J. Lee,[4] M. Sung,[4] C. White,[4] A. Wolf,[4] M.M. Zoeller,[4] X. Fu,[5] B. Nemati,[5] W.R. Ross,[5] P. Skubic,[5] M. Wood,[5] M. Bishai,[6] J. Fast,[6] E. Gerndt,[6] J.W. Hinson,[6] T. Miao,[6] D.H. Miller,[6] M. Modesitt,[6] E.I. Shibata,[6] I.P.J. Shipsey,[6] P.N. Wang,[6] M. Battle,[7] L. Gibbons,[7] S.D. Johnson,[7] Y. Kwon,[7] S. Roberts,[7] E.H. Thorndike,[7] T.E. Coan,[8] J. Dominick,[8] V. Fadeyev,[8] I. Korolkov,[8] M. Lambrecht,[8] S. Sanghera,[8] V. Shelkov,[8] T. Skwarnicki,[8] R. Stroynowski,[8] I. Volobouev,[8] G. Wei,[8] M. Artuso,[9] M. Gao,[9] M. Goldberg,[9] D. He,[9] N. Horwitz,[9] S. Kopp,[9] G.C. Moneti,[9] R. Mountain,[9] F. Muheim,[9] Y. Mukhin,[9] S. Playfer,[9] S. Stone,[9] X. Xing,[9] J. Bartelt,[10] S.E. Csorna,[10] V. Jain,[10] S. Marka,[10] D. Gibaut,[11] K. Kinoshita,[11] P. Pomianowski,[11] B. Barish,[12] M. Chadha,[12] S. Chan,[12] D.F. Cowen,[12] G. Eigen,[12] J.S. Miller,[12] C. O'Grady,[12] J. Urheim,[12] A.J. Weinstein,[12] F. Würthwein,[12] D.M. Asner,[13] M. Athanas,[13] D.W. Bliss,[13] W.S. Brower,[13] G. Masek,[13] H.P. Paar,[13] J. Gronberg,[14] C.M. Korte,[14] R. Kutschke,[14] S. Menary,[14] R.J. Morrison,[14] S. Nakanishi,[14] H.N. Nelson,[14] T.K. Nelson,[14] C. Qiao,[14] J.D. Richman,[14] D. Roberts,[14] A. Ryd,[14] H. Tajima,[14] M.S. Witherell,[14] R. Balest,[15] K. Cho,[15] W.T. Ford,[15] M. Lohner,[15] H. Park,[15] P. Rankin,[15] J.G. Smith,[15] J.P. Alexander,[16] C. Bebek,[16] B.E. Berger,[16] K. Berkelman,[16] K. Bloom,[16] T.E. Browder,[16*] D.G. Cassel,[16] H.A. Cho,[16] D.M. Coffman,[16] D.S. Crowcroft,[16] M. Dickson,[16] P.S. Drell,[16] D.J. Dumas,[16] R. Ehrlich,[16] R. Elia,[16] P. Gaidarev,[16] M. Garcia-Sciveres,[16] B. Gittelman,[16] S.W. Gray,[16] D.L. Hartill,[16] B.K. Heltsley,[16] S. Henderson,[16] C.D. Jones,[16] S.L. Jones,[16] J. Kandaswamy,[16] N. Katayama,[16] P.C. Kim,[16] D.L. Kreinick,[16] T. Lee,[16] Y. Liu,[16] G.S. Ludwig,[16] J. Masui,[16] J. Mevissen,[16] N.B. Mistry,[16] C.R. Ng,[16] E. Nordberg,[16] J.R. Patterson,[16] D. Peterson,[16] D. Riley,[16] A. Soffer,[16] P. Avery,[17] A. Freyberger,[17] K. Lingel,[17] C. Prescott,[17] J. Rodriguez,[17] S. Yang,[17] J. Yelton,[17] G. Brandenburg,[18] D. Cinabro,[18] T. Liu,[18] M. Saulnier,[18] R. Wilson,[18] H. Yamamoto,[18] T. Bergfeld,[19] B.I. Eisenstein,[19] J. Ernst,[19] G.E. Gladding,[19] G.D. Gollin,[19] M. Palmer,[19] M. Selen,[19] J.J. Thaler,[19] K.W. Edwards,[20] K.W. McLean,[20] M. Ogg,[20] A. Bellerive,[21] D.I. Britton,[21] E.R.F. Hyatt,[21] R. Janicek,[21] D.B. MacFarlane,[21] P.M. Patel,[21] B. Spaan,[21] and A.J. Sadoff[22]

(CLEO Collaboration)

[1]University of Kansas, Lawrence, Kansas 66045
[2]University of Minnesota, Minneapolis, Minnesota 55455
[3]State University of New York at Albany, Albany, New York 12222
[4]Ohio State University, Columbus, Ohio, 43210
[5]University of Oklahoma, Norman, Oklahoma 73019

[6]Purdue University, West Lafayette, Indiana 47907
[7]University of Rochester, Rochester, New York 14627
[8]Southern Methodist University, Dallas, Texas 75275
[9]Syracuse University, Syracuse, New York 13244
[10]Vanderbilt University, Nashville, Tennessee 37235
[11]Virginia Polytechnic Institute and State University, Blacksburg, Virginia, 24061
[12]California Institute of Technology, Pasadena, California 91125
[13]University of California, San Diego, La Jolla, California 92093
[14]University of California, Santa Barbara, California 93106
[15]University of Colorado, Boulder, Colorado 80309-0390
[16]Cornell University, Ithaca, New York 14853
[17]University of Florida, Gainesville, Florida 32611
[18]Harvard University, Cambridge, Massachusetts 02138
[19]University of Illinois, Champaign-Urbana, Illinois, 61801
[20]Carleton University, Ottawa, Ontario K1S 5B6 and the Institute of Particle Physics, Canada
[21]McGill University, Montréal, Québec H3A 2T8 and the Institute of Particle Physics, Canada
[22]Ithaca College, Ithaca, New York 14850

1. Introduction

This paper presents a preliminary CLEO analysis[1] of $b \to u\ell\nu$ decays to the exclusive final states $\pi\ell\nu$, $\rho\ell\nu$ and $\omega\ell\nu$. The ultimate goal of this analysis is to improve our knowledge of $|V_{ub}|$. ARGUS[2] and CLEO[3] have already demonstrated that $|V_{ub}| > 0$ by examining the inclusive lepton momentum spectrum from B decays at the $\Upsilon(4S)$. These experiments observe events with lepton momenta greater than 2.4 GeV/c, which is kinematically forbidden for the dominant $b \to c\ell\nu$ processes, but is still accessible to $b \to u\ell\nu$ decays. While these analyses clearly establish an excess in this endpoint region, and hence that $|V_{ub}| > 0$, extracting a reliable value of $|V_{ub}|$ is difficult because of the theoretical uncertainty in extrapolating from the observed rate in the endpoint region to the total $b \to u\ell\nu$ rate. Values of $|V_{ub}/V_{cb}|$ obtained from these analyses range from 0.07 to 0.11, with the theoretical uncertainty dominating.

An alternate route to $|V_{ub}|$ is through the study of exclusive $b \to u\ell\nu$ channels. The most precise previous information available for such channels is the upper limit set by CLEO[4] in the combined modes $\rho^-\ell^+\nu$, $\rho^0\ell^+\nu$ and $\omega\ell^+\nu$. The CLEO result corresponds to an upper limit of $\mathcal{B}(B^0 \to \rho^-\ell^+\nu) < 3.2 \times 10^{-4}$ at the 90% confidence level (ISGW model[5]).

The analysis presented here studies the two pseudoscalar modes $\pi^-\ell^+\nu$ and $\pi^0\ell^+\nu$, the three vector modes $\rho^-\ell^+\nu$, $\rho^0\ell^+\nu$ and $\omega\ell^+\nu$.[6] At a fixed $|V_{ub}|$, the existing form factor models predict a wide range of partial widths for these modes, as Table 1 shows. Unfortunately, measured branching fractions depend on the form factor model used to evaluate the experimental efficiencies, as does the extraction of $|V_{ub}|$. We therefore need to discriminate between the different models.

The ratio $\Gamma(B^0 \to \rho^-\ell^+\nu)/\Gamma(B^0 \to \pi^-\ell^+\nu)$ provides one means of discrimination. Because the $\pi\ell\nu$ rate is helicity-suppressed when the daughter meson is at rest in the B meson rest frame (at q^2_{max}), where the form factors for the decay are largest, while the $\rho\ell\nu$ rate is not, we expect the ratio to be larger than one. The exact value for the ratio will depend on the q^2 behavior of the form factors. In Table 1, we see that the predictions of the ratio span a fairly broad range.

2. Neutrino Measurement and Exclusive $b \to u\ell\nu$

Experimentally, semileptonic decays are troublesome because of the undetected neutrino. This analysis takes advantage of the excellent hermeticity and resolution of the CLEO

Table 1. Predictions for the exclusive partial widths $\Gamma(B^0 \to \pi^-\ell^+\nu)$ and $\Gamma(B^0 \to \rho^-\ell^+\nu)$ and the ratio $\Gamma(B^0 \to \rho^-\ell^+\nu)/\Gamma(B^0 \to \pi^-\ell^+\nu)$. The partial width units are $10^{12}|V_{ub}|^2$ sec^{-1}.

Model	$\Gamma(B^0 \to \pi^-\ell^+\nu)$	$\Gamma(B^0 \to \rho^-\ell^+\nu)$	$\Gamma(B^0 \to \rho^-\ell^+\nu)/\Gamma(B^0 \to \pi^-\ell^+\nu)$
WSB[7]	6.3 – 10.0	18.7 – 42.5	3.0 – 4.3
KS[8]	7.25	33.0	4.6
ISGW[5]	2.1	8.3	4.0
ISGW II[9]	9.6	14.2	1.5

detector located at the Cornell Electron Storage Ring (CESR) to obtain information about the neutrino in semileptonic $b \to u\ell\nu$ decays. Three concentric tracking devices provide a momentum resolution of $\sigma_p/p = 0.005 \oplus 0.0015p$ (p in GeV/c), while covering 95% of the 4π solid angle. The CsI calorimeter located inside of the CLEO solenoid provides an energy resolution well approximated by $\sigma_E/E = 0.019 + 0.0035/E^{0.75} - 0.001E$ (E in GeV), while covering 98% of 4π. The detector is described in detail elsewhere.[10] This analysis is based on a data sample with a luminosity of 2.46 fb^{-1} (2.64×10^6 $B\bar{B}$ decays).

The underlying idea is very simple: the $B\bar{B}$ system is produced at rest in CLEO and the beam energy is known very precisely, so we can measure the neutrino four momentum by measuring the missing energy and momentum of an event. We define

$$E_{miss} \equiv 2E_{beam} - \sum_i E_i \quad (1)$$

$$\vec{p}_{miss} \equiv -\sum_i \vec{p}_i, \quad (2)$$

where the index i runs over all charged tracks and all showers in the calorimeter that pass cuts designed to reject false tracks and spurious showers from hadronic interactions.

In events with no extra missing particles, $\vec{p}_{miss}$ can be reliably associated with the momentum $\vec{p}_\nu$ of the signal mode neutrino. The $b \to u\ell\nu$ decay can then be fully reconstructed: the energy difference $\Delta E \equiv E_{beam} - (E_h + E_\ell + |\vec{p}_\nu|)$, where h is the candidate hadron, should be zero, and the beam-energy constrained mass $M_B \equiv \sqrt{E_{beam}^2 - |\vec{p}_h + \vec{p}_\ell + \vec{p}_\nu|^2}$ should reconstruct at the B mass. Signal events without K_L^0's or extra neutrinos show resolutions of approximately 260 MeV on E_{miss} and 110 MeV on $|\vec{p}_{miss}|$.

Signal events with particles missing in addition to the neutrino usually fail the reconstruction criteria. Those background events that pass the criteria do so because they have extra particles missing. Consequently, we reject events with multiple leptons or a non-zero total charge because they indicate a second neutrino or a missed charged particle, respectively. Most remaining events with extra missing particles are eliminated by requiring that $M_{miss}^2 \equiv E_{miss}^2 - |\vec{p}_{miss}|^2$ be consistent with zero. The criterion $M_{miss}^2/2E_{miss} < 300$ MeV is used since the M_{miss}^2 resolution varies approximately as $2E_{miss}\sigma_{E_{miss}}$.

Continuum background is suppressed using standard event shape variables. We employ the event sphericity (characterized by the second Fox-Wolfram moment[11]) and the net momentum transverse to the momentum of the candidate lepton outside of forward and backward cones. $B\bar{B}$ events are in general more spherical and have a large transverse momentum compared to the jetty continuum events.

Both electrons and muons are used in this analysis. We combine information from specific ionization, energy/momentum measurements from the calorimeter and tracking systems, and position matching from these two systems to identify electrons down to 600 MeV/c. Muon candidates must register hits in muon counters at least 3 interaction lengths deep, limiting the muon momentum range to approximately 1.0 GeV/c. The probability that a hadron is misidentified as a lepton (a "fake lepton") is of the order 0.1% (1%) for electron (muon) identification. All identified leptons are used for purposes of the extra lepton veto. Candidate signal muons must additionally have registered in counters at least 5 interaction lengths deep. The $b \to u\ell\nu$ processes are enhanced over $b \to c$ by requiring the leptons to have momenta larger than 1.5 GeV/c (2.0 GeV/c) in the $\pi\ell\nu$ (vector) modes. The lower cut is used in the π modes because these modes are expected to have a softer lepton momentum spectrum.

A π^0 candidate must have a 2-photon invariant mass within 2 standard deviations (about 12 MeV) of the π^0 mass. Within any one of the five modes, we pick the meson candidate in each event that yields the smallest value of $|\Delta E|$.

The vector meson candidates are approached by examining the 2π and 3π invariant mass distributions. To help estimate the possible contamination of our samples by nonresonant $u\ell\nu$ decays, we have compared results from three different analyses of the distributions. The first analysis makes a simple cut on the 2π (3π) mass within 90 (30) MeV of the nominal ρ (ω) mass; the second employs a 2π (3π) mass sideband subtraction in the ρ (ω) modes, and the third fits the observed 2π and 3π mass distributions. These three approaches are described in detail in the following section. For the ω mode, we impose the additional requirement that the $\omega \to 3\pi$ decay lie within the central region of the Dalitz plot.

The dominant background in both the π and the vector modes comes from $B\bar{B}$ events in which there is at least one $b \to c\ell\nu$ decay and either an undetected K_L, a second neutrino, or both. Monte Carlo studies indicate that feed-across among the five modes contributes the next largest background. In the vector modes, $b \to u\ell\nu$ decays to higher mass final states result in a small background component. The backgrounds from fake leptons and from continuum processes are measured with the data and are small in every mode.

3. Extracting the yields

The general approach taken to determine the signal yields is to fit to the observed distribution of events in the $M_B - \Delta E$ plane in each of the five modes. The procedure used must address two issues. First of all, the feedacross background from the vector modes into the $\pi\ell\nu$ modes is non-negligible, but *a priori* we do not know the relative rate between these modes. By fitting the distributions in $M_B - \Delta E$ in the five reconstructed $b \to u\ell\nu$ modes simultaneously, the data in the vector modes constrains the $\rho\ell\nu$ background in the $\pi\ell\nu$ modes.

A more difficult challenge is posed by the nonresonant $u\ell\nu$ backgrounds to the vector modes, since we know neither the rate nor the shape that for this background. By using the observed $\pi\pi$ and 3π invariant mass distributions in the three ways mentioned above we show that this analysis has little or no contamination from nonresonant decays. The simplest method, simply cutting around the peak regions in the $\pi\pi$ and 3π mass regions, measures the sum of the resonant and nonresonant $u\ell\nu$ decays within the mass windows defined. The details of the general fitting procedure will also be introduced within the discussion of this analysis.

The second approach uses $\pi\pi$ and 3π mass sideband subtractions to minimize the sensitivity to any nonresonant component. Agreement both among variations in this approach and between this approach and the simple mass cut approach argue that the nonresonant contribution is small.

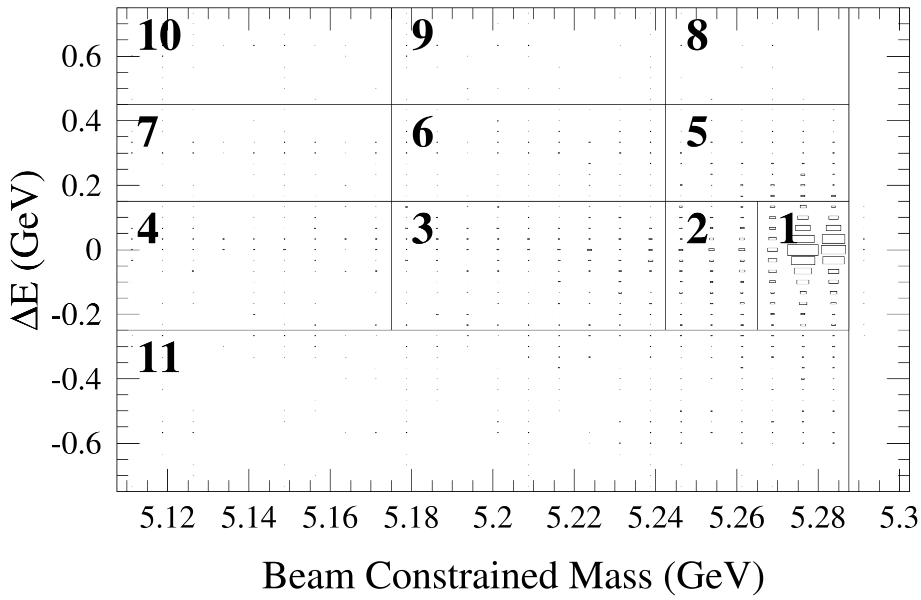

Fig. 1. Bins in $M_B - \Delta E$ Space

Finally, we will introduce the $\pi\pi$ and 3π mass distributions, changing the fitting procedure from a fit to the distribution in the $M_B - \Delta E$ plane to that in the 3 dimensional $M_B - \Delta E - \pi\pi(3\pi)$ space in the $\rho(\omega)$ modes. We will first demonstrate that the resonant component is sufficient to explain the observed observed distribution. We will then introduce different $\pi\pi\ell\nu$ samples into the fit to estimate how large a nonresonant contribution the observed distribution can tolerate.

3.1. Analysis with Simple $\pi\pi/3\pi$ Mass Cuts

For each of the five decay modes, for each event passing the previously-mentioned cuts, we compute M_B and ΔE. We obtain yields in 11 bins in $M_B - \Delta E$ space, as shown in Fig. 1. The signal peaks in Bin 1. The efficiency for signal to fall in Bin 1 is 2.9% for $\pi^-\ell^+\nu$, 1.9% for $\pi^0\ell^+\nu$, 0.8% for $\rho^-\ell^+\nu$, 1.4% for $\rho^0\ell^+\nu$, and 0.6% for $\omega\ell^+\nu$.

After subtracting the continuum and fake lepton backgrounds, we fit the $M_B - \Delta E$ distributions in our five reconstructed $b \to u\ell\nu$ modes simultaneously, 55 bins in all. In addition to the signal shapes and the feed-across shapes between the five modes, the fit includes $b \to c$ and other $b \to u\ell\nu$ background components. The relations $\frac{1}{2}\Gamma(B^0 \to \pi^-\ell^+\nu) = \Gamma(B^+ \to \pi^0\ell^+\nu)$ and $\frac{1}{2}\Gamma(B^0 \to \rho^-\ell^+\nu) = \Gamma(B^+ \to \rho^0\ell^+\nu) \approx \Gamma(B^+ \to \omega\ell^+\nu)$ constrain the neutral meson rates relative to the charged meson rates. We therefore obtain two yields, $N_{\pi^\pm\ell^\mp\nu}$ and $N_{\rho^\pm\ell^\mp\nu}$, from the fit.

The signal, $b \to c\ell\nu$ background and feed-across background distributions in M_B versus ΔE are obtained from a Monte Carlo simulation. The $b \to c$ decays are simulated as completely as possible, and the generated particle multiplicities and momenta spectra match the CLEO data quite well. For this preliminary analysis we have used signal event generators

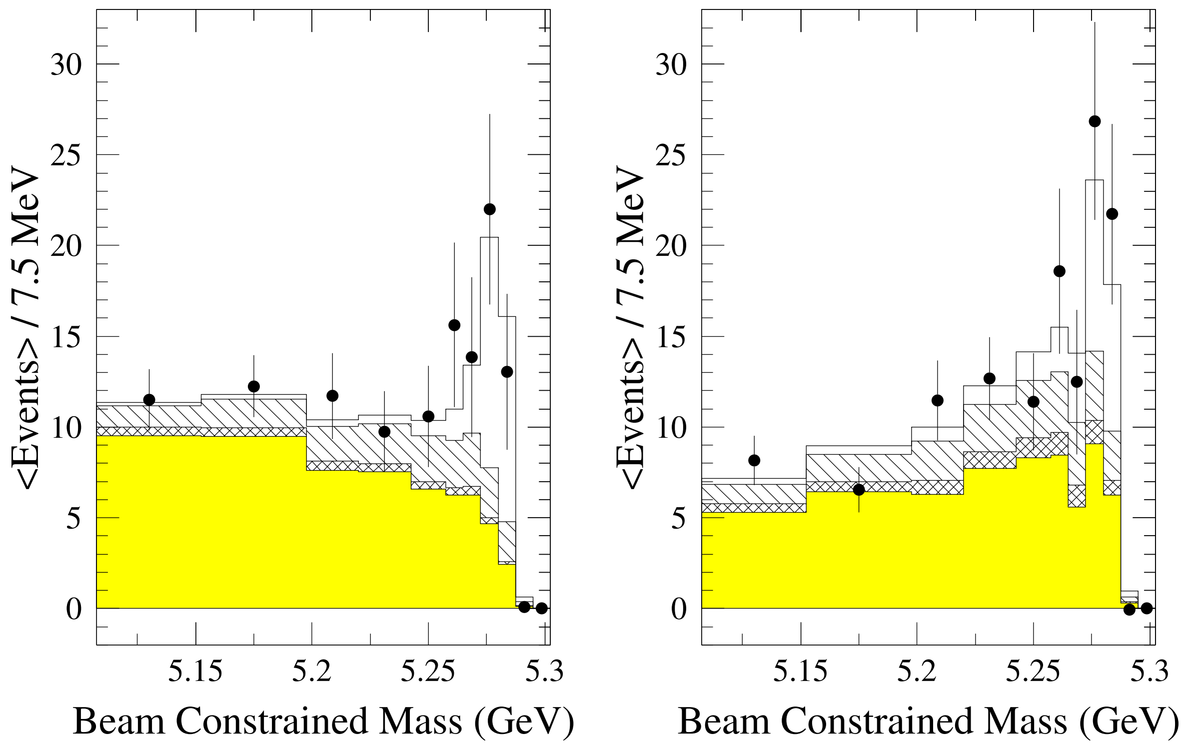

Fig. 2. Beam constrained mass distributions for the combined $\pi^-\ell^+\nu$ and $\pi^0\ell^+\nu$ modes (left) and the combined vector modes (right), for the analysis with simple $\pi\pi/3\pi$ mass cuts. The points are continuum- and fake-subtracted data. The histograms show the contribution from $b \to c$ (shaded), feeddown from higher mass $b \to u\ell\nu$ (cross-hatched), signal mode crossfeed (hatched) and signal (hollow).

based on the ISGW and WSB models. The model dependence of the results concerns only the predicted q^2 distributions. Polarization in the vector mode is varied by hand and included in the systematic uncertainty. The $b \to c\ell\nu$ background level is taken as a single fitting parameter, the same for all of the five modes, while the feed-across rates between the five modes are tied to the signal yields $N_{\pi^\pm\ell^\mp\nu}$ and $N_{\rho^\pm\ell^\mp\nu}$. Monte Carlo simulation also provides the $M_B - \Delta E$ distributions for the higher mass $B \to X_u\ell\nu$ backgrounds. The inclusive lepton yield at high momentum fixes this background level. We vary the physical model and the rate by hand to estimate the systematic uncertainty in this procedure.

Thus we fit 55 data points with 3 parameters: the $B^0 \to \pi^-\ell^+\nu$ rate; $B^0 \to \rho^-\ell^+\nu$ rate; and the $b \to c\ell\nu$ background scale factor. The fit just described finds a π^+ yield of 728 $\pm$ 195 events, a ρ^+ yield of 1183 $\pm$ 269 events, and a $b \to c$ scale factor of 1.06 $\pm$ 0.04. It has a χ^2 of 64.7 for 55 – 3 = 52 degrees of freedom. In Fig. 2 we compare the M_B distributions for the data and for the fit in the ΔE range -250 MeV $< \Delta E <$ 150 MeV (the ΔE signal band) in both the combined $\pi\ell\nu$ and the combined vector modes. A signal is apparent, both in $\pi\ell\nu$ and $\rho/\omega\ell\nu$. With the procedure just described, the $\rho/\omega\ell\nu$ yield includes both true $\rho/\omega\ell\nu$

and any nonresonant $\pi\pi/3\pi$ yield in the mass region, since we have *not* included low-mass nonresonant $\pi\pi/3\pi$ in our $b \to u\ell\nu$ background term.

3.2. Analysis with $\pi\pi/3\pi$ Mass Sideband Subtractions

One approach to eliminating nonresonant $B \to \pi\pi/3\pi\ell\nu$ background from the $B \to \rho/\omega\ell\nu$ signal is to perform an analysis that is identical to the one just described, but subtract $\pi\pi/3\pi$ mass sidebands from the yields for the vector modes. Using sidebands on either side of the mass peak that are each equal in size to the mass peak and displaced by one peak bin width, and assuming a linear shape, we find a π^+ yield of 705 ± 202 events, a ρ^+ yield of 1282 ± 369 events, a $b \to c$ scale factor of 1.07 ± 0.05, and a χ^2 of 64.9. This is in excellent agreement with the results from the simple cuts analysis. We have varied the location and width of the sidebands, and have also varied the sideband scale factor to allow for nonlinearity in the nonresonant $\pi\pi$ or 3π mass distribution. The results depend little on these variations. The beam-constrained mass distributions for the ΔE signal band, obtained using sideband subtractions, are shown in Fig. 3

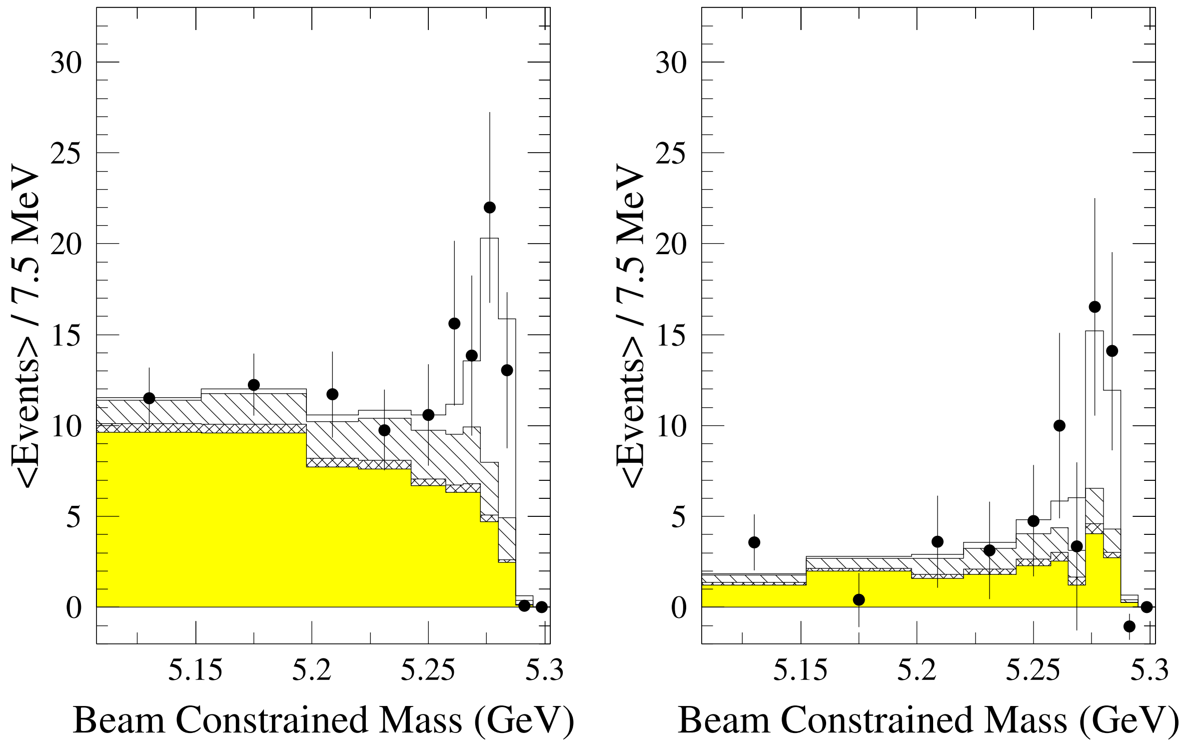

Fig. 3. Beam constrained mass distributions for the combined $\pi^-\ell^+\nu$ and $\pi^0\ell^+\nu$ modes (left) and the combined vector modes (right), for the analysis with $\pi\pi/3\pi$ mass sideband subtractions. The points are continuum- and fake-subtracted data. The histograms show the contribution from $b \to c$ (shaded), feeddown from higher mass $b \to u\ell\nu$ (cross-hatched), signal mode crossfeed (hatched) and signal (hollow).

3.3. Analysis Including the $\pi\pi/3\pi$ Mass Spectrum in the Fit

Because of the agreement between the results presented in the last two sections, one would expect that the $M_B-\Delta E-M_{\pi\pi/3\pi}$ distribution would be fit well without a nonresonant component. To determine over what region of the $M_B-\Delta E$ plane we would include the $\pi\pi/3\pi$ mass spectrum, we studied the Monte Carlo simulation of the vector modes. We found that the combinatoric component from signal events tended to peak broadly around the signal bin, so by default we include the mass spectrum in and nearby the signal region (excluding bins 4 and 7–10 in Fig. 1). As a systematic check we include the mass spectrum in all 11 bins.

We include the $\pi\pi$ mass distribution within the range ± 475 MeV of the nominal ρ mass (corresponding to 5 mass bins). The 3π mass distribution is included within the range $^{+150}_{-90}$ MeV of the nominal ω mass (4 bins). Higher masses can then be viewed as an unbiased indicator of the fit quality. As a systematic check, we also include 3 extra high mass bins in the ρ and ω modes.

Finally, to help minimize the systematic uncertainty in the simulation of the $b \to c\ell\nu$ background, we make use of the increased statistics of these fits and allow the $b \to c$ background scale to float independently in each of the five modes. This increases the number of fitting parameters from three to seven. As a systematic check, we restrict ourselves to one overall $b \to c$ scale factor.

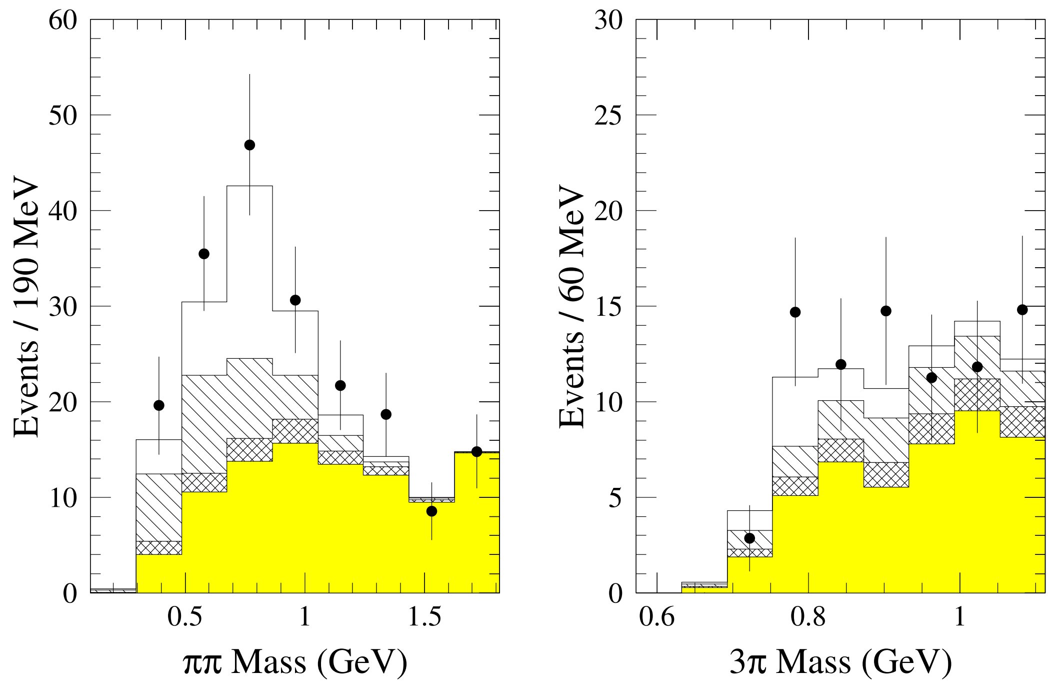

Fig. 4. $\pi\pi$ and 3π mass spectra for the $M_B - \Delta E$ signal bin. The fit given by the nominal fit is superimposed . For $\pi\pi$, we have summed $\pi^{\pm}\pi^0$ and $\pi^+\pi^-$. The shading is the same as in previous figures.

Table 2. Results of eight fits to data, using the $\pi\pi/3\pi$ mass spectra. Fits are for ("near"(6 bins) or "all"(11 bins) $M_B/\Delta E$ range) $\times$ (5 or 8 mass bins) $\times$ (1 or 5 $b \to c$ background scale factors). The preferred fit is "near"$\times 5 \times 5$.

$M_B/\Delta E$ range	near	near	near	near
Mass bins	five	five	eight	eight
$b \to c$ scales	one	five	one	five
$\pi^+\ell\nu$ yield	759 $\pm$ 181	708 $\pm$ 183	794 $\pm$ 180	744 $\pm$181
$\rho^+\ell\nu$ yield	1084 $\pm$ 184	1202 $\pm$ 189	1027 $\pm$ 171	1105 $\pm$174
$b \to c$ scale factor	1.03 $\pm$ 0.04	–	1.03 $\pm$ 0.03	–
$\pi^+\ell\nu$	–	1.08 $\pm$ 0.05	–	1.08 $\pm$ 0.05
$\pi^0\ell\nu$	–	1.18 $\pm$ 0.09	–	1.18 $\pm$ 0.09
$\rho^+\ell\nu$	–	0.92 $\pm$ 0.06	–	0.96 $\pm$ 0.06
$\rho^0\ell\nu$	–	0.98 $\pm$ 0.06	–	1.01 $\pm$ 0.05
$\omega\ell\nu$	–	0.96 $\pm$ 0.08	–	0.96 $\pm$ 0.06
χ^2	125.4	117.0	160.5	153.2
D.o.F.	121 – 3	121 – 7	175 – 3	175 – 7
$M_B/\Delta E$ range	all	all	all	all
Mass bins	five	five	eight	eight
$b \to c$ scales	one	five	one	five
$\pi^+\ell\nu$ yield	768 $\pm$ 181	719 $\pm$ 182	808 $\pm$ 179	749 $\pm$181
$\rho^+\ell\nu$ yield	1048 $\pm$ 173	1064 $\pm$ 174	986 $\pm$ 159	990 $\pm$159
$b \to c$ scale factor	1.04 $\pm$ 0.03	–	1.03 $\pm$ 0.02	–
$\pi^+\ell\nu$	–	1.09 $\pm$ 0.05	–	1.09 $\pm$ 0.05
$\pi^0\ell\nu$	–	1.19 $\pm$ 0.09	–	1.20 $\pm$ 0.09
$\rho^+\ell\nu$	–	0.97 $\pm$ 0.05	–	1.00 $\pm$ 0.04
$\rho^0\ell\nu$	–	1.08 $\pm$ 0.04	–	1.10 $\pm$ 0.03
$\omega\ell\nu$	–	0.93 $\pm$ 0.05	–	0.94 $\pm$ 0.03
χ^2	175.1	162.9	263.7	244.5
D.o.F.	176 – 3	176 – 7	275 – 3	275 – 7

Table 2 summarizes the results of our preferred fit and of the 7 fit variants obtained from the different combinations of the systematic checks described above. All of the fits have respectable χ^2's, and all give similar answers. The 5 independent $b \to c$ scale factors agree very nicely. The $\pi\pi$ and 3π mass spectra for the $M_B - \Delta E$ signal bin is shown in Fig. 4, with the results of our preferred fit superimposed.

3.4. Nonresonant $B \to \pi\pi/3\pi\ell\nu$

The sideband subtraction fits changed their yields negligibly when we varied the sideband subtraction scale factor by $\pm 30\%$. This argues against there being any significant

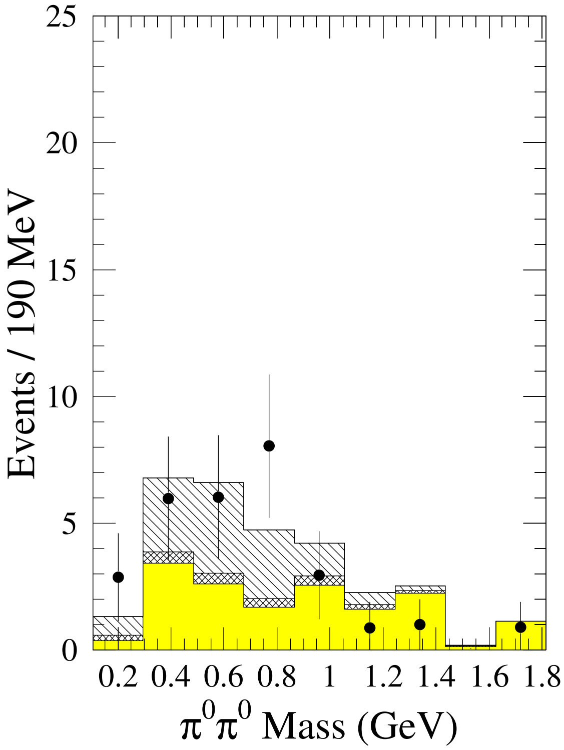

Fig. 5. $\pi^0\pi^0$ mass distribution obtained for the $M_B - \Delta E$ signal bin when analyzing the data for the $B \to \pi^0\pi^0\ell\nu$ mode. The histograms are the standard histograms (but with no signal component), and the nominal fit from Section 3.3 is used.

nonresonant $B \to \pi\pi/3\pi\ell\nu$ background. Similarly, the good quality of the fits when the mass spectra are included argues against any significant background having been omitted.

The smallness of the nonresonant $B \to \pi\pi/3\pi\ell\nu$ rate is not surprising. Following the quark-level process $b \to u\ell\nu$, with a spectator $\bar{u}$ or $\bar{d}$ quark, the final hadronic state must have isospin 0 or 1. Since isospin is conserved in the hadronization process, the $\pi\pi$ system can have only these values. For a $\pi\pi$ system with $I = 0$, the orbital angular momentum must be even. The $\pi^+\pi^-$ rate is twice the $\pi^0\pi^0$ rate, and the $\pi^\pm\pi^0$ rate vanishes. For a $\pi\pi$ system with $I = 1$, the orbital angular momentum must be odd. The $\pi^+\pi^-$ rate is half the $\pi^\pm\pi^0$ rate, and the $\pi^0\pi^0$ rate vanishes. A measurement of the $\pi^0\pi^0$ rate thus gives the $\pi^+\pi^-$ rate for even l. One expects that the $l = 1$ state near the ρ mass is ρ. One further expects that $l \geq 3$ states will be unimportant. Thus it is *only* a nonresonant $\pi^+\pi^-$ background that might be expected, and its size can be constrained by a measurement of the $\pi^0\pi^0$ rate.

We have carried out our analysis procedure looking for the $B \to \pi^0\pi^0\ell\nu$ mode. The $\pi^0\pi^0$ mass distribution for the $M_B - \Delta E$ signal bin is shown in Fig. 5. The histograms are the standard histograms (but with no signal component), and the nominal fit from Section 3.3 is used. Note that the fit parameters are determined without the inclusion of the $\pi^0\pi^0$ data – Fig. 5 shows a zero-parameter fit. The observed $B \to \pi^0\pi^0\ell\nu$ rate is fully explained by known, existing components. There is no need for, and very little room for, any true $B \to \pi^0\pi^0\ell\nu$.

We have introduced a nonresonant $B \to \pi\pi\ell\nu$ component into the fitting procedure. The $\pi\pi$ mass spectrum is taken from a spectator model calculation, and has a broad peak centered just below the ρ mass. A true $I = 0$ $\pi\pi$ mass distribution would likely be flatter than the one we have used, so we obtain a conservative estimate of the influence of nonresonant $B \to \pi\pi\ell\nu$ from this treatment. In one fit we set $N_{\pi^+\pi^-} = 2N_{\pi^0\pi^0}$, $N_{\pi^\pm\pi^0} = 0$. In another, we set $N_{\pi^+\pi^-} = 2.2N_{\pi^0\pi^0}$, $N_{\pi^\pm\pi^0} = 0.4N_{\pi^0\pi^0}$, allowing for a small $I = 1$ component. In addition to the data previously included in the fit, we include the analysis for $B \to \pi^0\pi^0\ell\nu$. We constrain the $\pi^0\pi^0$ $b \to c$ scale factor to the average of the $b \to c$ scale factors for the three vector modes.

For the fit with the pure $I = 0$ $B \to \pi\pi\ell\nu$ sample, the central value for the $B \to \rho\ell\nu$ yield changes little, but it develops asymmetric errors, 1162^{+233}_{-317} events, vs. 1202 ± 189 events with no nonresonant component. For the fit with the $I = 1$ admixture, the yield is 1058^{+315}_{-367}.

Our conclusion from all these investigations is that there is no evidence for nonresonant $B \to \pi\pi\ell\nu$. Unless it mimics $B \to \rho\ell\nu$ in shape more than the spectator model distribution we have used, its influence on the $B \to \rho\ell\nu$ rate introduces an error of at most +0%, -20%.

4. Systematic Errors

The changes in fitted yield due to reasonable variations in the mix of $D/D^*/D^{**}$ assumed for $b \to c\ell\nu$ in the $B\bar{B}$ Monte Carlo ($\pm$ 30% variations) are small, being $\pm$ 50 events for $B \to \pi\ell\nu$ and $\pm$ 20 events for $B \to \rho\ell\nu$. The changes due to $\pm$50% variations in the amount of high mass $b \to u\ell\nu$ assumed in the Monte Carlo are also small, $\pm$20 events for $B \to \pi\ell\nu$ and $\pm$90 events for $B \to \rho\ell\nu$. Systematic errors from variations in the assumed decay of the second B in the event and from the detector simulation have also been investigated, by carrying out variations in K^0_L fraction, charm semileptonic decay branching fraction, charged particle and photon finding efficiencies, false charged particle and false photon rejection effieiencies, charged particle momentum resolution, and photon energy resolution. The systematic uncertainties are summarized in Table 3.

As a check, we use the technique of full reconstruction with "measured" neutrino to measure the branching fraction for $B \to D^{*\pm}\ell^{\mp}\nu$ via the modes $D^{*+} \to \pi^+ D^0$, $D^0 \to K^-\pi^+$. We find that the simulation of E_{miss}, $\vec{p}_{miss}$, ΔE and M_B agrees well with the data (Figure 6), and that $\mathcal{B}(B^0 \to D^{*-}\ell^+\nu) = 4.66 \pm 0.65\%$. This agrees with the published CLEO result[12] of $4.49 \pm 0.32 \pm 0.39\%$, which used a higher statistics technique.

5. Results and Conclusions

The lepton momentum spectra for the $M_B - \Delta E$ signal bin for $B \to \pi\ell\nu$ and $B \to \rho/\omega\ell\nu$ are shown in Fig. 7. The spectra obtained from the data are quite stiff, with a sizeable fraction of events beyond the $b \to c\ell\nu$ endpoint. The sum of the signal and background distributions, scaled according to the fit results, shows good agreement with the data.

For $B \to \pi\ell\nu$, the $V-A$ interaction predicts that the angle between the lepton and the vector opposite the π momentum in the W rest frame, $\theta^*_{\pi\ell}$, should have a $\sin^2\theta^*_{\pi\ell}$ distribution.

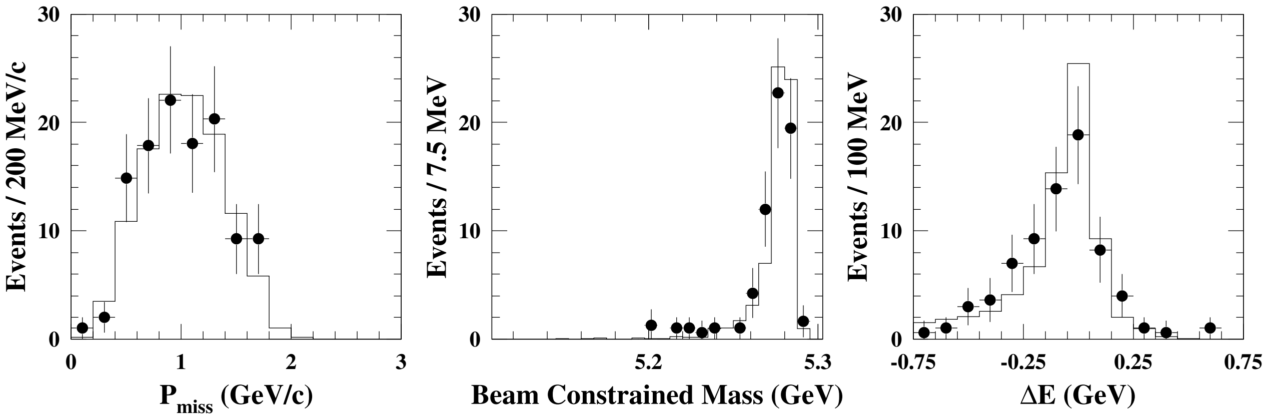

Fig. 6. $|\vec{p}_{miss}|$ spectrum (left) M_B distribution (center) and ΔE distribution (right) for $D^{*\pm}\ell^{\mp}\nu$ reconstruction. The points are continuum and combinatoric background-subtracted data. The histograms are signal Monte Carlo distributions normalized to equal area.

For $B \to \rho/\omega\ell\nu$, the details of the angular distribution depend on the form factors, but a forward peaking in $\cos\theta^*_{\rho\ell}$ is expected. The observed $\cos\theta^*_{\pi\ell}$ and $\cos\theta^*_{\rho\ell}$ distributions, shown in Fig. 8, are in good agreement with these expectations.

Our preferred fit among the many we have performed is the one that includes the $\pi\pi/3\pi$ mass spectra, uses five $\pi\pi/3\pi$ mass bins, uses them only in the region in $M_B - \Delta E$ space near the signal bin, and allows five independent $b \to c$ background scale factors. With this fit we have a $B^0 \to \pi^-\ell^+\nu$ yield of 708 $\pm$ 183 events, and a $B^0 \to \rho^-\ell^+\nu$ yield of 1202 $\pm$ 189 events. Dividing by 2 (for μ and e), and by 2.64×10^6 (the number of neutral B's),

Table 3. Summary of systematic uncertainties in the $\pi\ell\nu$ and $\rho\ell\nu$ modes, and in the ρ/π ratio.

	$\pi\ell\nu$	$\rho\ell\nu$	ρ/π ratio
$D/D^*/D^{**}$	$\pm$5.5%	$\pm$1.7%	$\pm$5.2%
$b \to u\ell\nu$ feeddown	$\pm$2.4%	$\pm$8.2%	$\pm$10.6%
Detector simulation and second B	$\pm$18.0%	$\pm$18.0%	$\pm$24.2%
ρ/ω polarization	$\pm$5.0%	$\pm$14.0%	$\pm$19.0%
$b \to u\ell\nu$ crosstalk	$\pm$3.0%	$\pm$7.0%	$\pm$5.0%
nonresonant $\pi\pi$	–	+0%, -20%	+0%, -20%
lepton finding	$\pm$2.0%	$\pm$2.0%	$\pm$2.0%
lepton fakes, cont. BG	$\pm$6.0%	$\pm$6.0%	$\pm$6.0%
luminosity	$\pm$2.0%	$\pm$2.0%	$\pm$0.0%
Total, excluding nonresonant $\pi\pi$	$\pm$20.9%	$\pm$26.1%	$\pm$33.9%

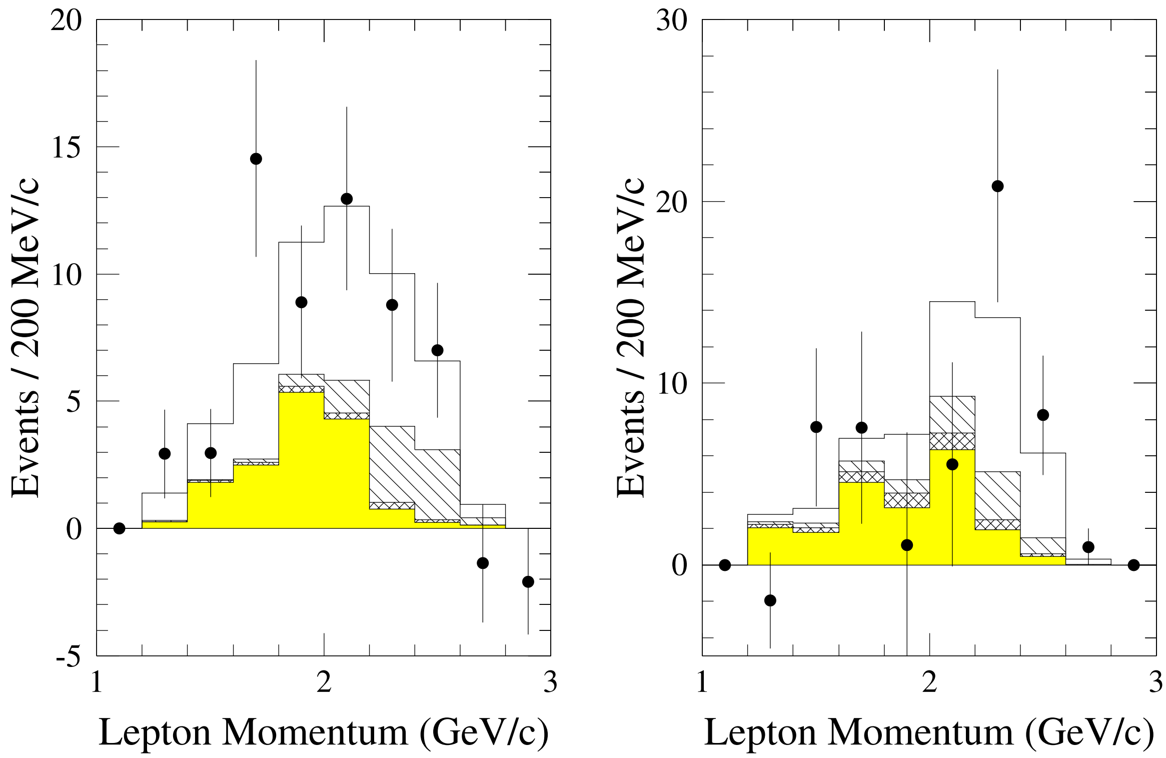

Fig. 7. Charged lepton spectrum for the combined $\pi^-\ell^+\nu$ and $\pi^0\ell^+\nu$ modes (left) and for the combined vector modes (right) The points are continuum-, fake-, and sideband-subtracted data. The top histogram is the total prediction using rates from the mass spectra fit, with components $b \to c$ (shaded), feeddown from higher mass $b \to u\ell\nu$ (cross-hatched), signal mode crossfeed (hatched) and signal (hollow).

we obtain branching ratios:

$$\begin{aligned}\mathcal{B}(B^0 \to \pi^-\ell^+\nu) &= (1.34 \pm 0.35 \pm 0.28) \times 10^{-4}, \\ \mathcal{B}(B^0 \to \rho^-\ell^+\nu) &= (2.28 \pm 0.36 \pm 0.59^{+0.00}_{-0.46}) \times 10^{-4},\end{aligned}$$

The first errors is statistical, the second is systematic, and the third, where given, is the uncertainty from a nonresonant $\pi\pi$ contribution. The ρ/π ratio is:

$$\frac{\Gamma(B^0 \to \rho^-\ell^+\nu)}{\Gamma(B^0 \to \pi^-\ell^+\nu)} = 1.70^{+0.81}_{-0.50} \pm 0.58^{+0.00}_{-0.34}.$$

These results were obtained using the ISGW model for $B \to \pi\ell\nu$ and $B \to \rho/\omega\ell\nu$ decays. If instead we use WSB, we find:

$$\begin{aligned}\mathcal{B}(B^0 \to \pi^-\ell^+\nu) &= (1.63 \pm 0.46 \pm 0.34) \times 10^{-4}, \\ \mathcal{B}(B^0 \to \rho^-\ell^+\nu) &= (3.88 \pm 0.54 \pm 1.01^{+0.00}_{-0.78}) \times 10^{-4}, \\ \frac{\Gamma(B^0 \to \rho^-\ell^+\nu)}{\Gamma(B^0 \to \pi^-\ell^+\nu)} &= 2.39^{+1.18}_{-0.69} \pm 0.81^{+0.00}_{-0.48}.\end{aligned}$$

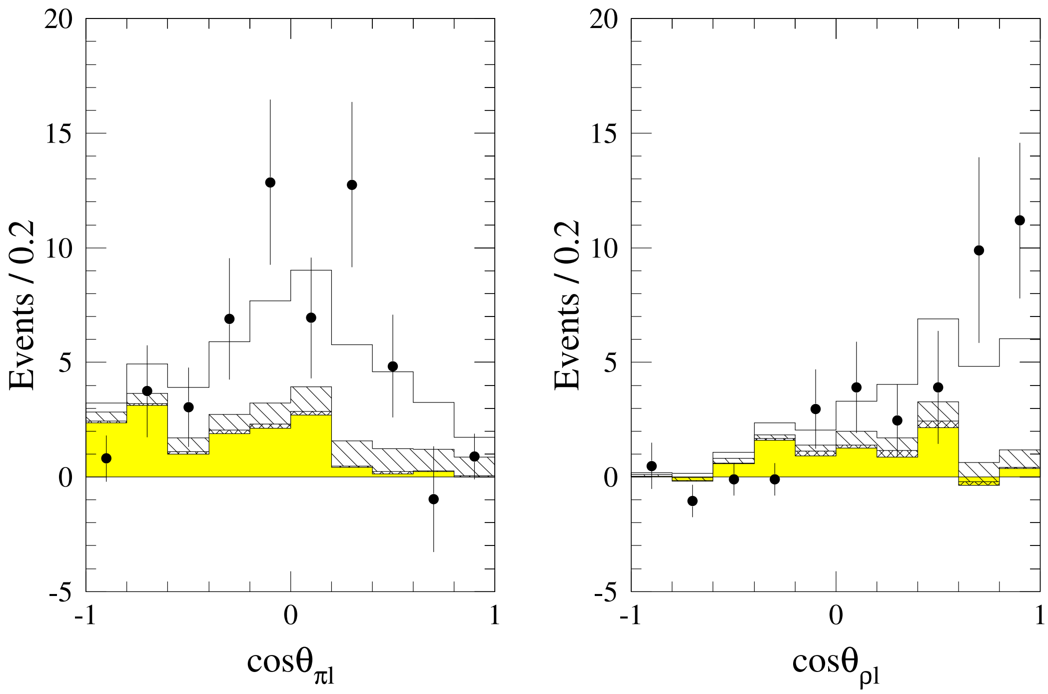

Fig. 8. (left) $\cos\theta^*_{\pi\ell}$ distribution for the combined $\pi^-\ell^+\nu$ and $\pi^0\ell^+\nu$ modes. (right) $\cos\theta^*_{\rho\ell}$ distribution for the combined vector modes. The points are continuum-, fake-, and sideband-subtracted data. The top histogram is the total prediction using rates from the mass spectra fit, with components $b \to c$ (shaded), feeddown from higher mass $b \to u\ell\nu$ (cross-hatched), signal mode crossfeed (hatched) and signal (hollow).

The ratio of rates found using the ISGW model is inconsistent with the large ratio predicted by that model (see Table 1). The ratio found using the WSB model is consistent with that model. A more careful evaluation of model dependence is needed before any precise statement about V_{ub} can be obtained.

These first measurements of exclusive $b \to u\ell\nu$ branching fractions signal the beginning of a new era for the determination of V_{ub}. Improvements in these measurements, in model calculations and lattice calculation will provide useful information for extracting new values for V_{ub}. Techniques developed in this analysis are also being applied to inclusive $b \to u\ell\nu$ analyses in the hopes of obtaining a more model-independent inclusive determination of V_{ub} as well.

6. Acknowledgments

We gratefully acknowledge the effort of the CESR staff in providing us with excellent luminosity and running conditions. This work was supported by the National Science Foundation, the U.S. Department of Energy, the Heisenberg Foundation, the Alexander von Humboldt Stiftung, the Natural Sciences and Engineering Research Council of Canada, and the A.P. Sloan Foundation.

7. References

1. A preliminary analysis focusing on $\mathcal{B}(B^0 \to \pi^- \ell^+ \nu)$ was presented at XXXth Rencontres de Moriond: L. Gibbons, University of Rochester preprint UR1427, 1995, *to appear in* Proceedings of the XXXth Rencontres de Moriond "Electroweak Interactions and Unified Theories", Les Arcs, France, March, 1995.
2. H. Albrecht *et al.* (ARGUS collaboration), Phys. Lett. **B234**, 409 (1990); *Ibid*, Phys. Lett. **B255**, 297 (1991).
3. R. Fulton *et al.* (CLEO collaboration), Phys. Rev. Lett. **64**, 16 (1990); J. Bartelt *et al.* (CLEO collaboration), Phys. Rev. Lett. **71**, 4111 (1993).
4. A.Bean *et al.* (CLEO collaboration), Phys. Rev. Lett. **70**, 2681 (1993).
5. N.Isgur, D.Scora, B.Grinstein and M.Wise, Phys. Rev. **D39**, 799 (1989).
6. Charge conjugate modes are implied.
7. M.Wirbel, B.Stech and M.Bauer, Z. Phys. **C29**, 637 (1985).
8. J.G.Körner and G.A.Schuler, Z. Phys. **C38**, 511, (1988).
9. N.Isgur and D.Scora, CEBAF preprint CEBAF-TH-94-14.
10. Y. Kubota *et al.* (CLEO collaboration), Nucl. Instrum. Methods Phys. Res. Sect. A **320**, 66 (1992).
11. G. Fox and S. Wolfram, Phys. Rev. Lett. **41**19781581.
12. B. Barish *et al.* (CLEO collaboration), Phys. Rev. **D51**, 1014 (1995).